Testing metals in tension and relaxation at elevated temperatures

Michel Darrieulat, Asdin Aoufi, Christophe Desrayaud

▶ **To cite this version:**

Michel Darrieulat, Asdin Aoufi, Christophe Desrayaud. Testing metals in tension and relaxation at elevated temperatures. Archives of Mechanics, 2023, 75 (1-2), pp.75 à 106. 10.24423/aom.4276 . emse-04114175

HAL Id: emse-04114175

https://hal-emse.ccsd.cnrs.fr/emse-04114175v1

Submitted on 1 Jun 2023

HAL is a multi-disciplinary open access archive for the deposit and dissemination of scientific research documents, whether they are published or not. The documents may come from teaching and research institutions in France or abroad, or from public or private research centers.

L'archive ouverte pluridisciplinaire **HAL**, est destinée au dépôt et à la diffusion de documents scientifiques de niveau recherche, publiés ou non, émanant des établissements d'enseignement et de recherche français ou étrangers, des laboratoires publics ou privés.

Distributed under a Creative Commons Attribution 4.0 International License

ARCHIVES OF MECHANICS
Arch. Mech. **75** (1-2), 75–106, 2023, DOI: 10.24423/aom.4276

Testing metals in tension and relaxation at elevated temperatures

M. DARRIEULAT, A. AOUFI, CH. DESRAYAUD

Mines Saint-Etienne, Université de Lyon, CNRS, UMR 5307 LGF, Centre SMS, F – 42023 Saint-Etienne France, e-mail: darrieulat@emse.fr

This article describes an apparatus for testing viscoplastic metallic alloys in tension at temperatures up to 400°C. Its distinctive feature is a two-shelled furnace which encompasses the test-piece. The extensometer is attached to the shoulders of the specimen and remains outside the oven, so that it works at room temperature. The strain ε_{rs} in the reduced section inside the tight fitting oven is calculated with the help of a finite element software from the strain ε_{ext} given by the extensometer. In the elastic range, the set-up was used for the measurement of Young's moduli. In the plastic and viscoplastic ranges, it was used to draw work-hardening curves and to perform relaxation tests representative of in-service conditions. In this later case, a method to derive the strain rate sensitivity from the decrease with time of the registered stress is presented. The furnace can be easily machined in a mechanical workshop for all shapes and dimensions of test-pieces, so that it can be adapted to various studies of the workability of metallic alloys, especially those which necessitate a rapid rise and precise maintenance in temperature.

Key words: tension testing, viscoplasticity, work hardening, engineering strain, extensometer, relaxation tests, strain rate sensitivity, elevated temperatures.

Copyright © 2023 The Authors.
Published by IPPT PAN. This is an open access article under the Creative Commons Attribution License CC BY 4.0 (https://creativecommons.org/licenses/by/4.0/).

1. Introduction

Tensile tests are useful to characterize the mechanical properties of the metals (yield strength, work-hardening modes etc.) and to study damage and fracture [1]. They ignore friction problems, so cumbersome when specimens stick to the anvil in compression at elevated temperatures, as documented by Montheillet and Desrayaud [2]. Numerous universal tensile testing machines, either hydraulic or electromagnetically powered, are available on the market. To heat the specimens, some additional gear (sometimes homemade) has to be mounted on the test-rigs.

The heating systems are mainly of three types and based on:

– Volume heating: an electric current crosses the specimen, which is heated by the Joule effect. This is the specificity of the Gleeble^{TM} machines. They allow rapid rises in temperature (several hundreds of degrees per second).

Fabrègue *et al.* [3] have taken advantage of this in the study of microstructural transformations.

– Induction: the specimen is heated by the eddy currents produced by a high frequency alternating current in an induction coil. A few turns of wire are wound around the test-piece. It works with ferromagnetic steels but also with other metals. An example of realization is given in Codrington *et al.* [4].

– Contact: the specimen is surrounded by a hot or warm atmosphere (air or inert gas against oxidation), in a furnace or in a climatic chamber. The heating energy is provided by electrical resistances under 600°C and by radiative rods through the reflection on the walls of the oven for higher temperatures. It is the best as regards the homogeneity in temperature of the specimen. That is why it is recommended by the ASTM E21 Standard *Test Methods for Elevated Temperature Tension Tests of Metallic Materials* [5].

All these devices must be compatible with some way of measuring the deformation of the specimen. The displacements of the crossbars can be known accurately, for example by using Linear Variable Differential Transformers (LVDT); but the rig yields under the load so it is better to measure the displacement on the specimen itself. Several techniques are available:

– Contact strain measurement techniques include strain gauges. Their attachment to the test-piece may be affected by temperature and some expertise is needed to correct the deviations caused by thermal expansion.

– Contact measurement also encompasses a wide range of extensometers. Some are specially designed for high temperatures, featuring alumina or silicon carbide extensions to keep the transducer away from the heated zone. Part of them has to lie outside the furnace.

– Non-contact strain measurement techniques: the heating gear must be provided with a glass window to follow the deformation of the specimen. This is the way the change in the form of a test-piece placed in a furnace was quantified at 1300°C [6]. Digital Image Correlation (DIC) techniques allow to determine complete strain fields, provided that oxidation does not blur the marks on the metal. Luong *et al.* [7] showed their feasibility up to 700°C with a speckle pattern deposited on a titanium specimen.

The present article features a tensile testing apparatus in which the central part of the specimen is heated by electrical resistances. The furnace is a two-shelled oven which encloses the test-piece. The extensometer is placed outside the furnace. The set-up was devised and machined in the LGF (Laboratoire Georges Friedel) of Saint-Etienne (France) which specializes in the deformation at temperature of metallic alloys. It can work in tension, stress relaxation and in complex tests including sequences of both changes of strain rate and temperature. All these tests are described in Lemaitre and Chaboche [8, pp. 256 et seq].

The paper is organized as follows. Section 2 offers a description of the appliance. Section 3 investigates the use of the apparatus in the elastic range, determines Young's moduli and discusses the accuracy of the measurements. Section 4 deals with the plastic and viscoplastic ranges with two applications: the determination of work-hardening curves when the apparatus is used in tension and the measurement of strain rate sensitivities when relaxation tests are performed. The conclusions try to assess the qualities and drawbacks of the appliance. The Appendix presents in detail the method used to calculate strain rate sensitivity from the decrease with time of the stress which maintains constant the deformation of the test-piece.

2. Design of the appliance

As it is stressed later, this section presents the set-up for a particular sheet type specimen. It can be adapted to other dimensions and other cases (plates, cylindrical test-pieces, rods, bars, pipes).

Mechanical set-up

Figure 1 pictures the apparatus. The testing machine is a hydraulic powered Instron^{TM} 1186 with a capacity of 200 kN. The holding system consists of two serrated wedge grips in contact over about 36 mm with the shoulders of the specimen. The later, machined out of a 4 mm thick sheet, is shown in Fig. 2.

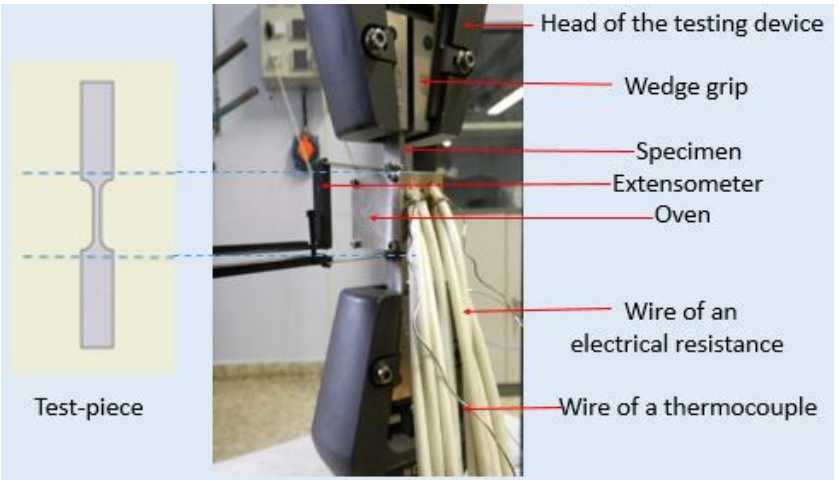

FIG. 1. Global view of the appliance.

It features shoulders 16 mm wide. The reduced section has a square cross area of 4 mm in side and is 24 mm long. The fillet radius is 6 mm. This geometry

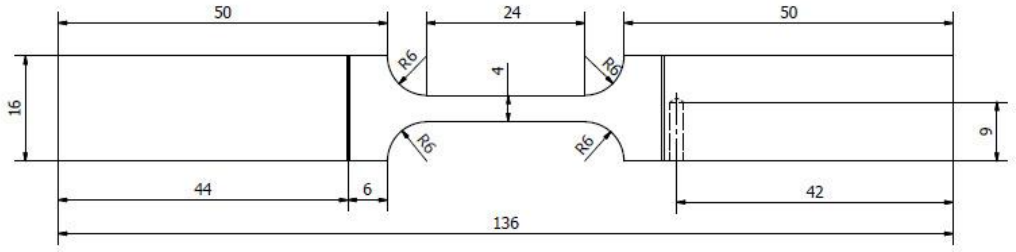

Fig. 2. Rectangular tension test-piece used in the experiments.

has been especially studied for the sake of homogeneity in temperature of the central part. Two gauge marks have been drawn on the shoulders for the knives of an extensometer to fit into. Close to one of them, a hole has been drilled to place a 4^{th} thermocouple outside the furnace. So the extensometer measures the elongation of a piece of material initially 48 mm long, 4 mm thick, whose width varies from 16 to 4 mm.

The material chosen for the subsequent calculations and experiments was a 2024 T3 aluminum, the composition of which is given in Table 1. This alloy is widely used for aircraft structures because of its good machinability. It has been hot-rolled into a 4 mm thick sheet, solution treated, quenched, levelled and submitted to natural ageing. Its measured hardness is 125 HV5.

Table 1. Chemical composition of the 2024 alloy in wt%.

Cu	Mn	Mg	Fe	Si	Al
4.4%	0.6%	1.5%	0.5%	0.3%	balance

Heating system

The oven consists of two halves shown in Fig. 3. When screwed together, these two shells encompass the reduced section and the fillets but only the edges of the shoulders, as detailed in Fig. 2. Four electrical resistances are set into the holes of each half of the furnace. The grooves which appear in Fig. 3 between the electrical resistances allow to insert three thermocouples.

The four resistances can raise the temperature to 400°C in only 40 s followed by a holding time of five minutes, as appears in Fig. 4. The data were recorded every second. The maintenance at the set-point value was ensured by the upper and lower thermocouples. Once the temperature is stabilized, the difference between them is of the order of one degree, due to the symmetry of the appliance.

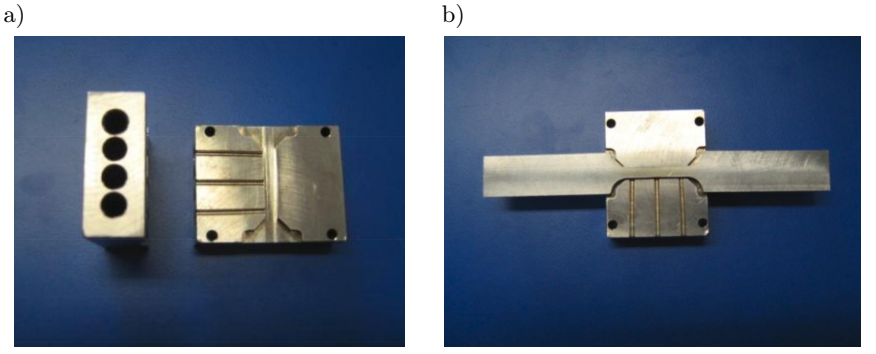

FIG. 3. Design of the furnace: a) front and inner side views of one half oven, b) fitting of the test-piece into it.

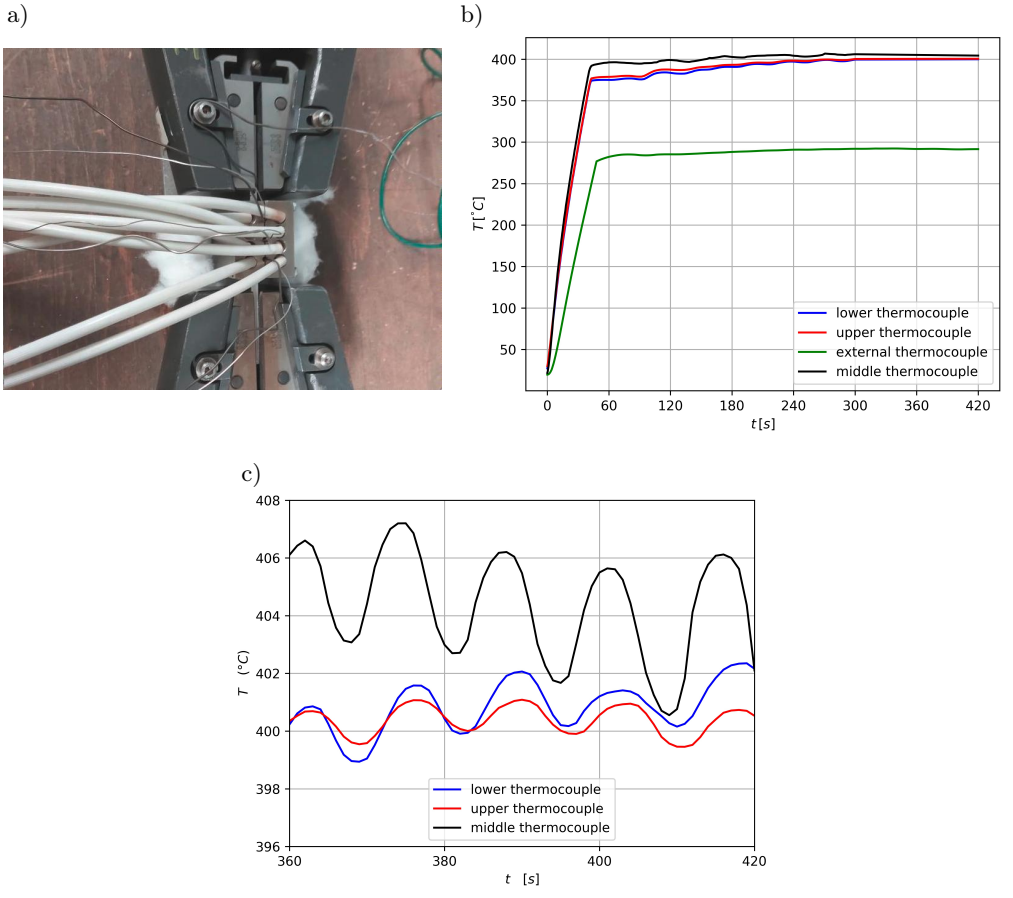

FIG. 4. Rise and stabilization of the temperatures in the oven: a) disposition of the thermocouples, b) curves $T(t)$ within the furnace and outside it, c) magnification of the readings of the framed box of inset b).

The middle thermocouple was not linked to the PID system. Its record has also been reported in the figure. An enlargement of the three curves in the stabilized zone (last minute of the recording) is shown in inset c).

The 4th thermocouple inserted in one of the heads of the specimen shows that the temperature falls rapidly outside the furnace. Figure 4 pictures its evolution, parallel to what happens inside the oven, but with much damped oscillations and some one hundred °C below.

Figure 4 prompts the following comments:

– oscillations: during the raise in temperature, there are no oscillations since the system works at full power. The oscillations correspond to the activation of the electrical resistances by the PID control. They affect the thermocouples simultaneously, as can be seen in the inset c);

– in the stabilized zone, they are roughly periodical with a period of about 15 s. Their amplitude depends on the sensitivity of the PID regulation. In the present experiments, the temperature of the 'Upper' and 'Lower' thermocouples varied of about 1.5°C around its mean value. The oscillations of the 'Middle' one are more than double (around 3.5°C);

– since heat flows at the ends of the oven, there is a parabolic profile of temperatures within it, hence the difference between the 'Upper' and 'Lower' recordings on one hand, the 'Middle' one on the other. The difference is a function of the heat flow. It is maximum when a maximum of power is injected in the system, at the end of the rise in temperature. After 40 s of heating it reaches 22°C. Then it decreases to 4°C in the stabilized zone.

The standard ASTM E21 specifies at least two thermocouples for a reduced section of less than 50 mm and a variation in temperature of less than the 3°C between them. In the present experiment, it lacks one degree to meet these requirements at approximately 39 mm in the immediate vicinity of the electrical resistances. Heating more slowly or maintaining intermediate temperature levels could improve this performance.

It was thought of interest to have not two measurements, but a full temperature map of the phenomenon. This required a finite element calculation which serves later for mechanical considerations, since the constitutive law of the material is temperature-dependent.

The specifications for the F.E. simulations were as follows:

– it was performed with the Abaqus^{TM} software (version 6.20);

– because of the variations in width of the test-pieces and the loss of heat at the contact with the wedge grips, a 3D analysis was deemed necessary. Axis 1 was chosen as the direction of tension, axis 2 for width, axis 3 for thickness. Only the steady state was considered since it is achieved before starting the tests;

– continuum 3D elements C3D8 were used (brick elements with 8 nodes and linear integration). The mesh was uniform and the cubic elements about one millimeter in size (four of them in the thickness);

– thermal boundary conditions: between the electrical resistances, the set point temperature was imposed on the four faces of the specimen. It ranged between 20 and 400°C. The thermal conductivity of the 2024 T3 alloy was taken as $\lambda = 147\,\mathrm{W/(m \cdot K)}$.

The temperature of the wedge grips was set at $T = 20°\mathrm{C}$, for the massive heads of the testing machine showed no sign of heating. On the surfaces of the shoulders, on which they grip, which are 16 mm wide and about 36 mm long, the heat transfer coefficient of $2000\,\mathrm{W/(m^2 \cdot K)}$ was introduced. On the surfaces which are in contact with the air, where there are neither oven or grips, the heat transfer coefficient was set to $25\,\mathrm{W/(m^2 \cdot K)}$. Only one eighth of the specimen was modelled due to the symmetries, the fixed point being at its center.

The results of the simulation are shown in Fig. 5 drawn at $T = 400°\mathrm{C}$ for clarity's sake. The temperature varies little with the width and the thickness, so

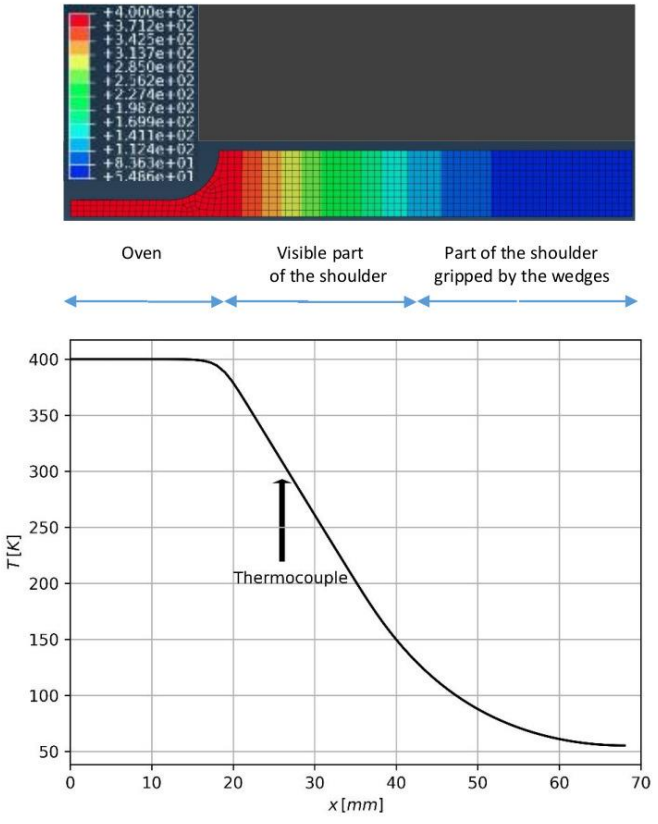

FIG. 5. Decrease in temperature along axis 1.

only the large, flat side of the specimen appears in the upper inset of the figure. The evolution of the temperature along axis 1 is plotted in the lower inset.

Figure 5 pictures the map of temperatures in the median plane of the test-piece. It does not change along axis 2 so that the decrease along axis 1 contains all useful information. The F.E. simulation was done by taking values of the literature for the heat transfer coefficients (25 and 2000 $\mathrm{W/[m^2 \cdot K]}$). Adjusting them would have required more thermocouple measurements and the fitter drilled only one of them in the test-piece. Nevertheless, the agreement between the simulations and the recordings is reasonable, as shown in Table 2. The important point is that the decrease in temperature outside the oven is gradual.

Table 2. Temperatures calculated and measured by the 4^{th} thermocouple.

Set point T [°C]	100	200	300	400
Measured T	71	148	222	291
Calculated T	80	156	232	309

Extensometer

The distinctive feature of the present appliance is the position of the extensometer, which is set entirely outside the furnace. In the literature, the authors found an example of tensile tester in which the central part of the test-piece is heated while its heads are cold gripped [9].

However, it uses high temperature extensometers directly attached to the gage length of the specimen. The extensometers have ceramic extensions which penetrate inside the oven while the rest is kept outside. This necessitates drilling slits in the walls of the furnace, which introduces a dissymmetry in the gear. The consequence is that it takes time to achieve a steady thermal state.

The conditions in which the extensometer works are as follows. Its legs locate its main body at about 10 mm off the furnace, in the open air of the laboratory where the radiation due to the small oven hardly rises the temperature. For the present experiments, the extensometer was an Instron™ n° 2620-604. It is designed to work between – 80 and 200°C and measures the displacements with an uncertainty of 1 μm. Only its knives are in contact with the heads of a test-piece. As can be seen in Fig. 5, the temperature at these spots may rise up to 300°C, but the legs, made of stainless steel, are thin and poor heat conductors.

Once the thermal steady state is obtained, the extensometer has to be calibrated for each temperature. It is positioned symmetrically with respect to the furnace, so that there is no thermal gradient between the knives.

Now, due to the heat, elongation takes place in the test-piece. According to Fig. 2, at room temperature, the distance between the knives is 48 mm,

although there is some tolerance in the machining of the housings. With aluminum alloys, the expansion coefficient is $23\times10^{-6}/°C$ (more than most metals), so that at 400°C the elongation reaches 0.4 mm. The question arose whether this had to be taken into account when calculating engineering strains (displacement divided by an initial length). At 400°C, the discrepancy is 0.87%, less than the uncertainty of the measurements (see Subsection 3.2). For the sake of simplicity, in this paper the strain measured by the extensometer was specified as the displacement divided by 48 mm at all temperatures.

One of the reasons of the design of the present apparatus is the commitment to a tight fitting furnace with rapid, homogeneous heating. If the strain in the heated part of the specimen cannot be reached in direct mode, it can be deduced from the readings of the extensometer, as shown in Sections 3 and 4.

3. Extensometry in the elastic range

As soon as in 1955, THOMAS and CALSON [10] performed tensile and creep tests placing the knives of their extensometer on the shoulders of their test-pieces, because oxidation limited the effective life of attachment fixtures. By optical extensometry, they spotted the contrasted deformations of the shoulders, filets and reduced section. Now that finite element software is available, it is possible to quantify all this and to predict what happens inside the oven.

In order to measure strains, the first investigation was to check that the presence of the furnace does not perturb the results of the mechanical tests. Indeed, when screwed together, its two halves allow some clearance between them and the specimen. Two tests were performed up to fracture at room temperature with the same crosshead speed. Special care was taken to the alignment of the test-piece and the heads of the testing machine. In the first test, only the test-piece was placed between the grips. In the second, the test-piece bore the fully geared furnace, but electricity was not turned on. The measured displacements were exactly the same.

3.1. Elastic deformation of the specimen

The specimen is designed to undergo a homogeneous deformation in its reduced section. This was checked by a F.E. simulation done with the Abaqus^{TM} Software used in the previous section. The runs were performed on the 2024 T3 aluminum alloy at $T = 20°C$, 200°C and 400°C. The elastic limits were set, respectively, at 345 MPa, 138 MPa and 20 MPa. Young's moduli were 72.5 GPa, 70.4 GPa and 68 GPa, hence maximum elastic deformations of 4.75×10^{-3} (20°C), 1.96×10^{-3} (200°C) and 0.30×10^{-3} (400°C).

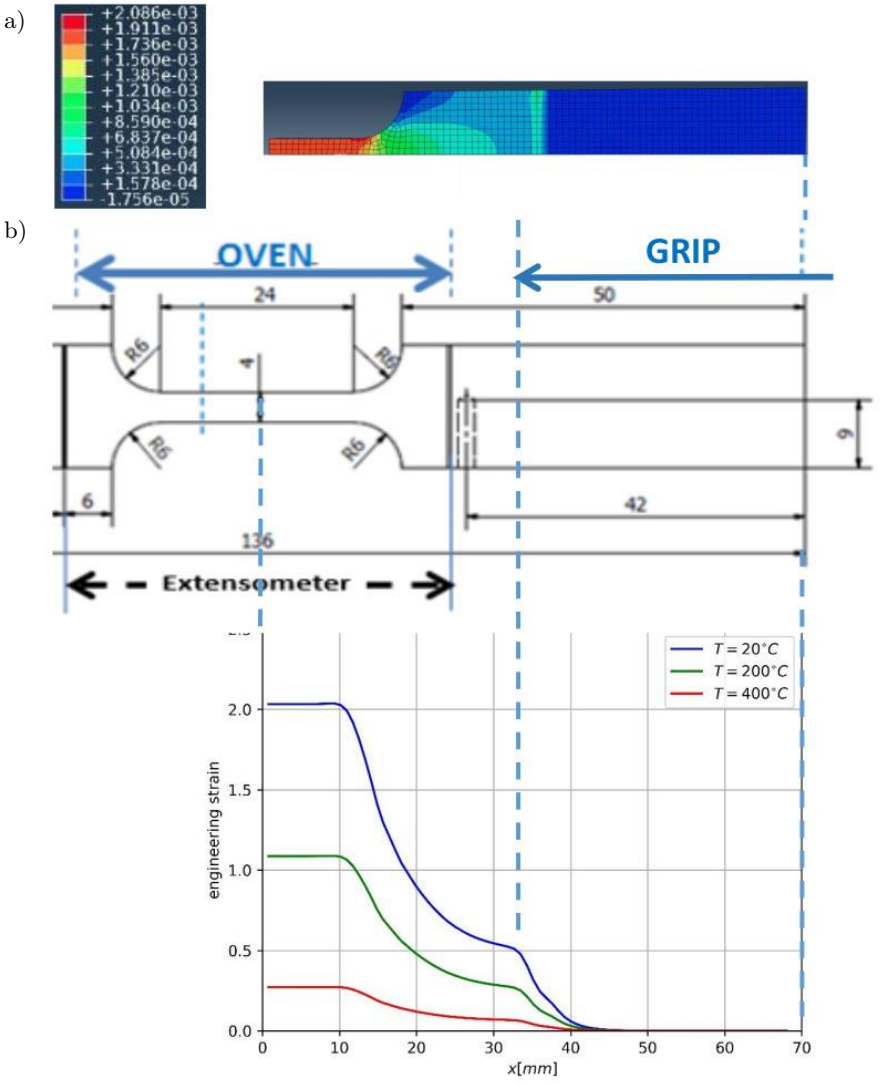

Fig. 6. Strain in the test-piece according to F.E. simulations; a) distribution of EE11 in the median plane of the test-piece at 20°C, b) EE11 along axis 1 at three temperatures.

Among the local strain outputs proposed by Abaqus^{TM}, the total strain E and its elastic part EE were chosen. EE11 is the component along axis 1. Its distribution in the median plane appears in Fig. 6 at room temperature for the conventional elastic strain of 2×10^{-3}.

In the fillets, the strain varies along axis 2 and the edge at the junction of the fillet and the shoulder is nearly unaffected by the deformation. No shear

was found in the thickness of the specimen. The evolution of EE11 along axis 1 appears in Fig. 6b at three temperatures for various elastic strains: in the three cases, the evolution is of the same type. In the reduced section, the total length of which is $12 \times 2 = 24$ mm, the strain is constant at 20 mm. The standard deviation of the nodes such as $x < 10$ mm is of the order of 10^{-7} at room temperature and 10^{-8} at 400°C. Then EE11 drops smoothly in a parabolic form up to the spot where the grip comes into contact with the head. At this point, EE11 drops sharply and becomes almost zero for $x > 43$ mm, leaving 25 mm of strain-free shoulder.

To account for the global deformation of the test-pieces, engineering strains were chosen as follows:

– ε_{ext} (extensometer) is the engineering strain obtained by dividing the displacement of one of the grooves of the test-piece by $L_0 = 24$ mm which is its initial distance to the center of the specimen (see Fig. 2). For that, 44 nodes meshing the cross section situated under the groove were considered, their displacements averaged and divided by 24 mm (only one eighth of the specimen is entered in the software because of the symmetries). These displacements were examined in various thermo-mechanical conditions and they were always found to be quite close. Even far in the plastic range the difference between them does not exceed half a μm, that is less than the resolution of the extensometer;

– ε_{rs} (reduced section) is the engineering strain obtained as follows eight nodes such as $x \approx 10$ mm were chosen in the cross section. They feature the groove of a virtual extensometer which stands for the one which cannot be placed on the reduced section because of the tight fitting furnace ε_{rs} is obtained by averaging the eight displacements and dividing by $l_0 = 10$ mm.

The values of ε_{rs} as a function of ε_{ext} appear in Fig. 7.

In Fig. 7, the graphs of $\varepsilon_{rs} = f(\varepsilon_{ext})$ at the three considered temperatures are straight lines and their slopes are indistinguishable, though of course the extension of the elastic domain varies. This linearity is due to the elastic behavior and to the design of the test-piece. A least squares method gave the slope: 1.315.

Note: this 1.315 value was compared to the result of a one-dimensional analytical calculation in which the strain in the test-piece is supposed uniaxial. The calculation was performed at room temperature, case in which Young's modulus is uniform. With these hypotheses, the contribution of each section of the test-piece to the lengthening is inversely proportional to its width. The reduced section accounts for 24 mm, the shoulders within the grooves for $2 \times 6 \times 4/16 = 3$ mm. The contribution of each fillet could be calculated analytically as

$$\int_0^6 \frac{dx}{4 - \sqrt{3x - x^2/4}} = 4.172 \text{ mm}.$$

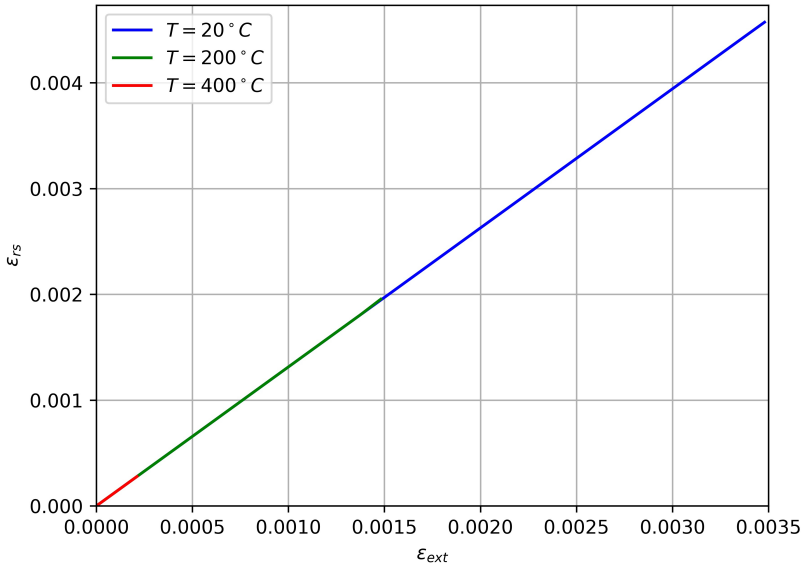

Fig. 7. Elastic range. Calculated strain in the reduced section ε_{rs} versus ε_{ext} strain measured by the extensometer for a 2024 T3 aluminum alloy at three temperatures.

The total is 35.344 mm, while the distance between the knives of the extensometer is 48 mm. This yields a slope $48/35.344 = 1.358$ instead of 1.315. This analytical checking of the results of the F.E. simulation puts in evidence the highly unidirectional character of the deformation in the test-piece.

3.2. Measurement of Young's moduli and assessment of their accuracy

The previous section has shown that in the elastic range, the strains throughout the test-piece can be calculated with the accuracy. This prompted to try and measure Young's moduli with the present appliance. They are required to perform F.E. simulations. Broadly speaking, they are available in the literature at room temperature and seldom above.

Young's moduli can be measured in a variety of ways. Ultrasonic resonance techniques are readily available at 20°C and specialised equipment can work at elevated temperatures. Impulse excitation techniques [11] are now commercially available. These are dynamic measurements, in opposition to the static measurements reported below.

The protocol used in the present experiments followed ASTM E111 *Standard Test Method for Young's Modulus, Tangent Modulus and Chord Modulus* [12]. The speed of the crossbar was set at $10^{-2}\,\mathrm{mm}\cdot\mathrm{s}^{-1}$. The materials were: the already described 2024 T3 alloy, an A304 stainless steel, Zircaloy-4 used for fuel cladding in nuclear reactors and a grade of brass containing one-third of zinc and

two-thirds of copper. Five temperatures were considered: 20°C, 100°C, 200°C, 300°C, 400°C. Preliminary tensile tests were performed to determine the intervals $[0, F_{max}]$ in which the deformation of the alloys is linear. F_{max} ranged from 6.7 kN for the stainless steel at room temperature down to 3.5 kN for aluminum at 400°C. Young's moduli were measured during unloading between F_{max} and $F_0 = 0.5$ kN. The displacements ranged from 61 μm (A304 at 400°C) to 137 μm (Zy-4 at 20°C).

Young moduli were calculated as $E = \frac{\sigma}{\varepsilon_{rs}}$ where $\sigma = \frac{\Delta F}{S_0}$, $S_0 = 16\,\text{mm}^2$, $\varepsilon_{rs} = 1.315\varepsilon_{ext}$, $\varepsilon_{ext} = \frac{\Delta l}{L_0}$ in which Δl is the elongation measured by the extensometer and L_0 the distance between its knives ($L_0 = 48$ mm). Figure 7 has shown that the ratio $\varepsilon_{rs}/\varepsilon_{ext}$ varies very little with temperature. It remained identical with other alloys in the subsequent F.E. simulations.

Hence, the accuracy of the measurements depends on:

– the force sensor. In the present experiments, it had a sensitivity of 10 N. A cell force of 20 kN was used, so that the loads were measured with an accuracy of the order of 10^{-3};

– the extensometer. This is the key point in the elastic range, since the displacements are small. Here, it had a sensitivity of 1 μm so the accuracy was of the order of 1 or 2%, an order of magnitude above the stresses.

The results are displayed in Fig. 8.

E is given in GPa and T in°C. The red bars indicate the uncertainty in the measurement.

Comments in Fig. 8

a) At room temperature, Young's modulus of aluminum 2024 was measured by ultrasounds at the LGF laboratory and the authors found E (20°C) = 72.6 GPa. This value was superior to the value they found with the present apparatus (E (20°C) = 66 GPa). Such discrepancies between mechanical and ultrasonic measurements have often been noted, see for example [12]. Instead of exact values at 20°C, difficult to obtain with mechanical gears, the most valuable piece of information yielded by the experiments under consideration is the decrease in temperature.

The results with the present aluminum sample appear in Fig. 6a. They are in good agreement with HOPKINS *et al.* [13] and MONDOLFO [14]. The decrease of $E(T)$ is approximately linear between 20 and 400°C, a phenomenon which is noted in the three following examples. The least squares methods applied to the experimental point yields:

$$E(T) = 66.7 - 0.037T \quad (E \text{ in GPa}, T \text{ in °C}). \tag{3.1}$$

b) The results for stainless steel A304 are reported in Fig. 6b. The moduli are two or three times larger than in other cases, hence the larger error bars.

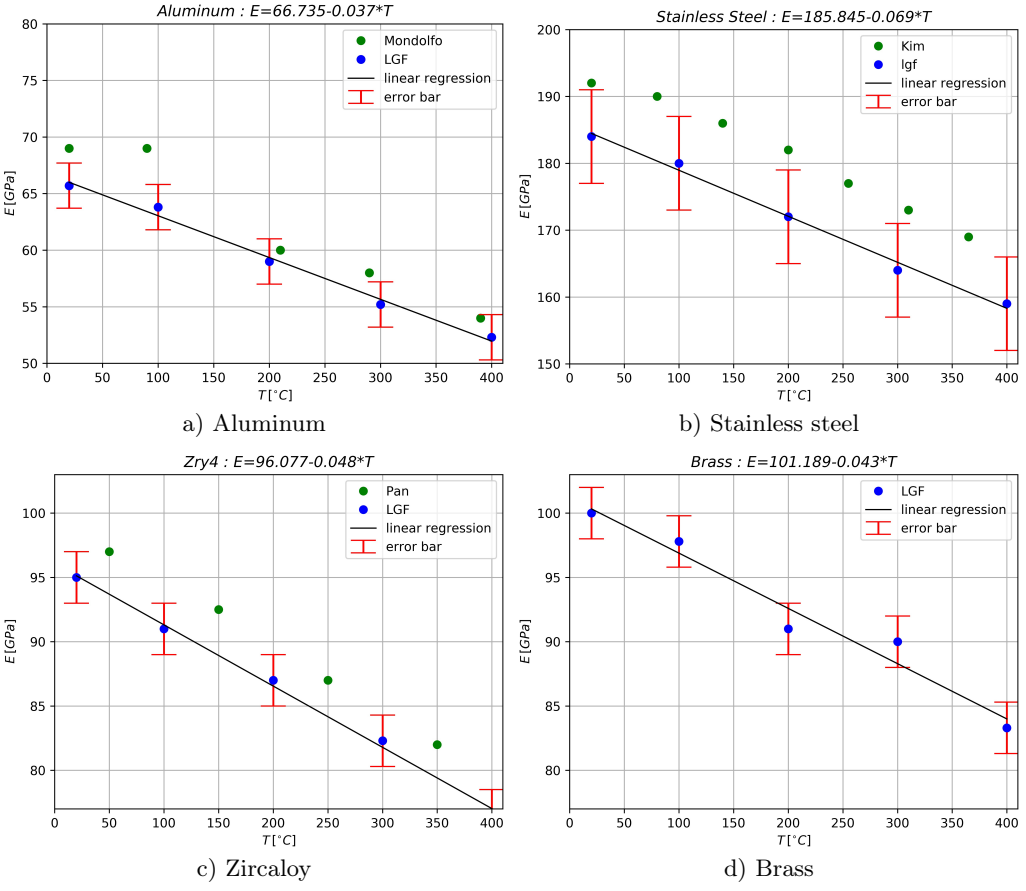

a) Aluminum b) Stainless steel

c) Zircaloy d) Brass

Fig. 8. Decrease of Young's moduli E with temperature for four metallic alloys.

The measures collected by Kim and *et al.* [15], have reported that the figure and their decrease is the same as the one found in the present experiment:

$$E(T) = 185.8 - 0.069T. \tag{3.2}$$

From another source [16, Fig. 26] the authors calculated $b = -0.075$. Such scatterings were found when they tried similar comparisons with the other alloys.

c) The Zircaloy-4 sample, provided by the CEZUS company, had been β-treated. Pan *et al.* [17] noted that the values of Young's moduli differ according to the heat treatment of the alloy: $E(T)$ decreases more rapidly in recrystallized alloys. Pan *et al.* results concerning alloys with Widmanstätten microstructures have been reported in Fig. 6c, along with those obtained by the present apparatus. This led to:

$$E(T) = 96.1 - 0.048T. \tag{3.3}$$

PAN *et al.* noted a strong dependence of $E(T)$ on the texture in these hexagonal, anisotropic metals. On the contrary, the composition of the alloy has little influence, as shown by NORTHWOOD *et al.* [18] who investigated various grades of alloyed zirconium, among which Zircaloy-2. To use the data of the literature, it is necessary to be documented on the heat treatments undergone by the material and it is not always the case.

d) Such a situation was encountered in the LGF laboratory with a brass alloy containing one-third of zinc and two-thirds of copper. The proportion between zinc and copper varies much among brass alloys, so that no data were available for this precise composition. The experiment gave $E = 100.3\,\text{GPa}$ at 20°C. As expected, it was intermediate between zinc ($E = 83\,\text{GPa}$) and copper ($E = 117\,\text{GPa}$). The decrease with temperature was:

$$E(T) = 101.2 - 0.043T. \tag{3.4}$$

The relation was needed for forming calculation. Other applications include the determination of the residual stresses which appear when metallic pieces are cooled and the search for values of the elastic constants required in the microscopic laws of behavior based on the mechanics of dislocations.

4. Extensometry in the plastic and viscoplastic ranges

For many metals, foremost aluminum, there is no precise limit between the elastic and the plastic ranges. Likewise, viscous phenomena appear progressively when the temperature is raised. It is the type of tests performed on the specimens which reveals these different aspects. In the first part of this section, the apparatus is used in tension for the drawing the work-hardening curves, plastic or viscoplastic as the case may be. Then it is used for relaxation tests which put in evidence the viscosity and allow the determination of strain rate sensitivities.

4.1. Determination of work-hardening curves

Whereas the elastic behavior of all metals is roughly linear, their work-hardening curves $\sigma(\varepsilon)$ have contrasted shapes although all increase monotonously up to some ultimate tensile strength. A priori, the relation between the strain ε_{rs} in the reduced section and the strain ε_{ext} given by the readings of the extensometer should be established for each material, temperature and velocity rate. Happily, things are simpler, as shown in the present subsection which successively:

– presents the experiments performed on the abovementioned 2024 T3 aluminum alloy,

– for the sake of comparison, repeats the corresponding calculations on stainless steel,

– discusses the use of the linear approximation $\varepsilon_{rs} = k\varepsilon_{ext}$ suggested by the above experiments in the case of other alloys.

Experiments on the 2024 T3 alloy

In the first place, the $\sigma(\varepsilon)$ behavior of the alloy was measured at room temperature on the apparatus described above. The curve was almost identical to the recordings of the supplier (French aluminum manufacturer Constellium). The latter also provided curves at various temperatures, which the authors used as an independent, experimental basis not relying on an external extensometer.

The work-hardening curves of the 2024 T3, obtained at a velocity rate of $\dot{\varepsilon} = 1.6 \times 10^{-3}\,\mathrm{s}^{-1}$, appear in Fig. 9a for strains up to 10%. After that, they are almost flat. The points entered as material behavior into the Abaqus^{TM} software are marked by round dots on the graph. The displacement applied to the grooves of the extensometer was 2.4 mm. This produced a strain of about 10% in the reduced section.

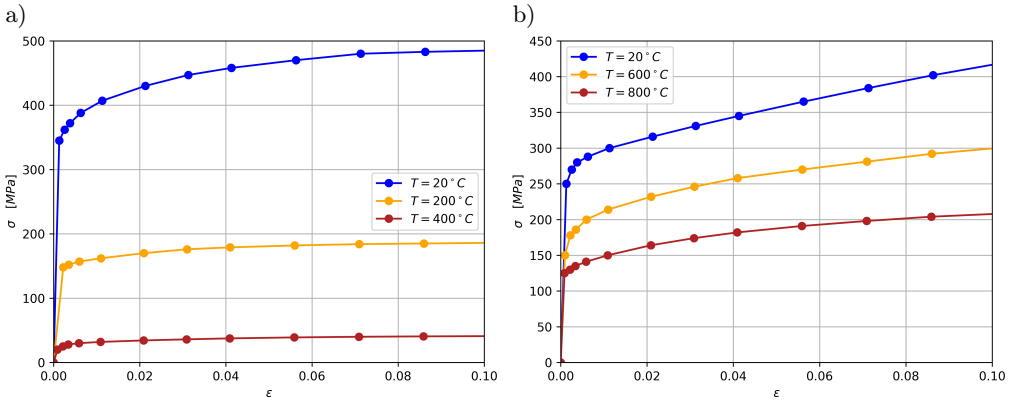

Fig. 9. Work-hardening curves for a) the 2024 T3 alloy ($T = 20°$, 200° and 400°C), b) the A 304 alloy ($T = 20$°C, 600°C and 800°C).

The strains ε_{ext} and ε_{re} were measured and calculated as in the elastic range, since the reduced section also deforms plastically in a homogeneous manner on $2 \times l_0 = 20$ mm. The values of ε_{rs} as a function of ε_{ext} appear in Fig. 10.

Figure 10a prompts the following comments:

– as a proof of the homogeneity of the deformation in the reduced section in the plastic range, the values of the total strain E strain of all the nodes such as $x < 10$ mm were collected. Their standard deviation was less than 1.5×10^{-3} up to 10%;

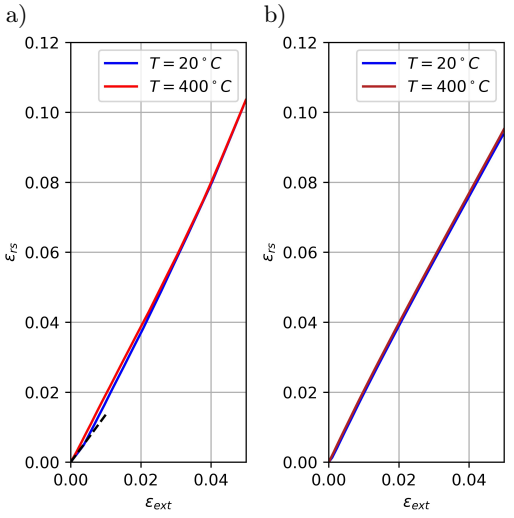

FIG. 10. Calculated strain in the reduced section versus strain measured by an extensometer placed outside the furnace: a) 2024 T3 aluminum alloy, b) A 304 stainless steel.

– temperature has little influence on the $\varepsilon_{rs} = f(\varepsilon_{ext})$ curves. The difference between 20°C and 400°C has a mean value of $\Delta\varepsilon = 1.1 \times 10^{-3}$ with a maximum of $\Delta\varepsilon = 2.2 \times 10^{-3}$. Three stages can be distinguished:

– in the elastic range, the slope is 1.315, as noted in Fig. 7. It appears as a dotted line in Fig. 10a. In Fig. 10, it appears distinctly only for the 2024 T3 alloy at 20°C; in the other cases, the elastic domain is too small,

– in the plastic (or viscoplastic) range the curve is close to a straight line. Nevertheless, in the case of the 2024 T3 alloy, it can be approximately divided into two parts:

– for $0.005 < \varepsilon_{ext} < 0.03$, the slope of the curve was found equal to 2.01 at 20°C and to 1.95 at 400°C by the least squares method. It can be noted that with the geometry of the present test-piece, the slope would be exactly 2 if the specimen had rigid shoulders and fillets and a deformable reduced section 24 mm long (see Fig. 2.),

– for $\varepsilon_{ext} > 0.03$, the slope of the curve rises slowly. In the $0.04 < \varepsilon_{ext} < 0.05$ interval it reaches 2.38 at 20°C and 2.34 at 400°C.

The strain maps provided by the Abaqus^{TM} post processor at each increment of calculation show that the transition around occurs when the deformation ceases in the shoulders and the fillets and concentrates in the reduced section. Were the test-piece made of a deformable gage length of 20 mm, all the rest being rigid, the slope would be $48/20 = 2.40$. That is almost the case at $\varepsilon_{ext} = 0.05$, when the work-hardening is close to zero.

Comparison with stainless steel

The previous section has shown that in the case of the 2024 T3 alloy, the relation between the strain in the reduced section and the strain given by the outer extensometer is piecewise linear, if not globally linear.

A few numerical simulations showed that varying the thermal parameters in the input data produced almost no change in the $\varepsilon_{rs} = f(\varepsilon_{ext})$ curves. Has the type of work-hardening more influence? In aluminum alloys, at large strains, $\sigma = f(\varepsilon)$ is rather flat. On the contrary, in stainless steels, the work-hardening curves exhibit a steady slope before reaching the ultimate tensile stress.

Hence, it was decided to repeat the calculations on the A 304 alloy used in Section 3.2. The data of work-hardening were taken from Lemaitre and Chaboche [8, page 165, fig. 1b] and appear in Fig. 9b. For the Abaqus^{TM} runs, Young's modulus was set to 191 GPa at 20°C and 135 GPa at 800°C. The thermal conductivity was set to $\lambda = 16$ W/(m.K). The corresponding $\varepsilon_{rs} = f(\varepsilon_{ext})$ curves appear in Fig. 10b.

Temperature has still less influence than in the case of aluminum, since the difference between 20°C and 400°C has a mean value of $\Delta\varepsilon = 0.8 \times 10^{-3}$ with a maximum of $\Delta\varepsilon = 1.1 \times 10^{-3}$. For $\varepsilon_{ext} < 0.03$, the slope of the curve is equal to 1.92 at all temperatures. It lowers to 1.82 when approaching $\varepsilon_{ext} < 0.05$. The difference with aluminum must be related to the fact that, in the case of stainless steel, work-hardening is strong up to $\varepsilon_{ext} = 0.05$. Thus the curve is closer to $\varepsilon_{rs} = 2\varepsilon_{ext}$ than in the case of the 2024 T3 alloy.

Validity of a linear approximation in the case of aluminum and stainless steel

It has already been pointed out that their onset, $\varepsilon_{rs} = f(\varepsilon_{ext})$ and $\varepsilon_{rs} = 2\varepsilon_{ext}$ differ since the slope is 1.315 instead of 2. Assessing the consequences of a global linear approximation on the resulting work-hardening curves implies to compare:

– the curves $\sigma = f(\varepsilon)$ entered in the software as representative of the true mechanical behavior of the material. It was assumed that they have been determined by the most accurate methods available. As mentioned above, the authors checked it in the case of aluminum at room temperature,

– the curves $\sigma = f(2\varepsilon_{ext})$ drawn from the readings of the extensometer and the cell force.

Six graphs, each picturing two curves, the original one and the one obtained with $\sigma = f(2\varepsilon_{ext})$, have been drawn for aluminum and stainless steel at room and elevated temperatures. In the six cases, they are quite close. The most illustrative may be that of the stainless steel at 800°C. Figure 11 pictures the difference between the original curve (the same which appears in red in Fig. 9b and the green one drawn with the $\varepsilon_{rs} = 2\varepsilon_{ext}$ assumption.

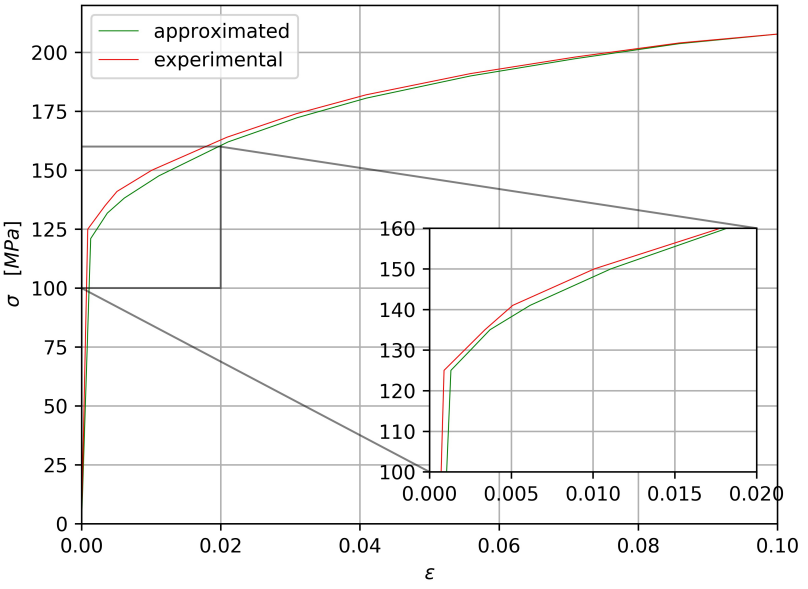

FIG. 11. Original work-hardening curve of A304 stainless steel at 800°C (in red) and curve drawn using the $\varepsilon_{rs} = 2\varepsilon_{ext}$ approximation (in green).

Figure 11 prompts the following comments:

– the main difference in the curves is found at the elastic-plastic transition zone and does not exceed 1.6 MPa, as seen in the inlet. After $\varepsilon > 0.05$ the curves are almost indistinguishable;

– the consequence for the representation of the transition zone can be better seen on the enlargement. For its introduction in the Abaqus^{TM} software, the experimental curve had to be drawn with an elastic limit chosen at 125 MPa, the corresponding strain being 0.6×10^{-3}. Now, the elastic strain in the reduced section is overestimated by the approximation $\varepsilon_{rs} = 2\varepsilon_{ext}$. This changes the elastic limit on the recalculated curve and it appears at 121 MPa. This is largely an artificial effect since in most alloys, including aluminum alloys and stainless steels, there is no sharp transition between the elastic and plastic domains. Nevertheless, setting a limit was required by the F.E. software;

– the difference between the two curves must be weighed against the uncertainties in the measurements of stress and strain. As seen above, for the stresses, the accuracy is around 10^{-3} beyond the elastic range. For strains, with the extensometer used in this paper, it decreases from $5 \cdot 10^{-3}$ at the end of the elastic range to less than 10^{-3} in the plastic range. This is the order of magnitude of the discrepancy shown in Fig. 11: 1.3% at the maximum in the elastic range, almost zero at $\varepsilon = 0.1$.

The ratio $k = \varepsilon_{rs}/\varepsilon_{ext}$ and its dependence on work-hardening

As shown by the following simulations, k is not always equal 2. First and foremost, it depends on the geometry of the tensile-test pieces. In most of them, at high strain, the deformation concentrates in the gauge length. So k is linked primarily to the ratio between the length of the reduced section and the distance between the knives of the extensometer. This ratio is equal to 2 in this paper but it would vary with other test-pieces and heating gears since the knives of the extensometer must be placed outside the furnace.

For the test-pieces used in this paper, the effect of various factors influencing the relation $\varepsilon_{rs} = f(\varepsilon_{ext})$ were examined. It began by the influence of the experimental conditions and of the material properties on the ratio k. Changes in the thermal parameters and boundary conditions had almost no consequence on the results of the F.E. simulations.

Changes in the strain rate vary the level of stress at elevated temperatures but do not cause much change in the form of the work-hardening curves. An example is given in [8, p. 255]. Increasing the strain rate from to 10^{-4}/min. to 2.5×10^{-2}/min when testing an Udimet nickel alloy roughly doubles the strain but not the characteristics of hardening.

Changes in the set-point temperature affect the level of the stress and the form of the hardening curve.

To distinguish between the effects of these two factors, F.E. simulations were made with work-hardening curves differing only in the elastic limit. The resulting $\varepsilon_{rs} = f(\varepsilon_{ext})$ relations in the plastic range were parallel lines, the offset between them has been due to the different extensions of the elastic ranges in which $\varepsilon_{rs} = 1.315\varepsilon_{ext}$.

This shows that the crucial factor influencing k is the form of the work-hardening curves. The latter relate to three main types:

a) after the linear elastic range, there is much work-hardening so that the ultimate tensile strength σ_{max} is well above the conventional σ_{el}. A typical example are austenitic stainless steels;

b) high stresses are reached elastically and there is a limited range of plastic deformation and even no plastic deformation at all. Steels with a high carbon content behave in that way;

c) once σ_{el} is reached, the stress keeps at a constant level for some time and then has a small increase, so that σ_{max} is not much higher than σ_{el}; such are unalloyed and mild steels.

A case has been investigated with aluminum and stainless steel. Extra simulations were made on the nickel alloy Udimet 720. Work-hardening curves at 20°C and 700°C were taken from Terzi [19, page 56]. They appear in Fig. 12a. The corresponding $\varepsilon_{rs} = f(\varepsilon_{ext})$ relations appear in Fig. 12b. The phenomena already

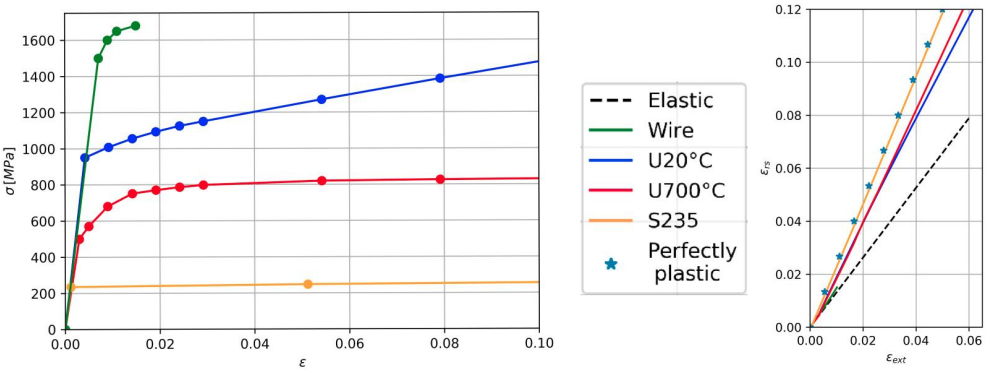

FIG. 12. Evaluation of the strain within the furnace in the case of various alloys: S 235, pre-tensioning wire, Udimet 720 at 20°C and 700°C. The limiting cases are elasticity and perfect plasticity; a) work-hardening curves, b) $\varepsilon_{rs} = f(\varepsilon_{ext})$ curves.

mentioned for aluminum and stainless steel are plainly visible: $\varepsilon_{rs} = f(\varepsilon_{ext})$ is close to a straight line; at room temperature, the calculated slope is 1.96, close to 2; at 700°C, with the flattening of the work-hardening curve, it raises slowly and reaches 2.14 for $0.07 < \varepsilon_{rs} < 0.12$.

Figure 12 also documents the results of the investigation of cases b and c:

– steel for pre-stressing wires was chosen as an example for case b. The corresponding $\varepsilon_{rs} = f(\varepsilon_{ext})$ curve could be fitted by $\varepsilon_{rs} = 1.538\varepsilon_{ext}$. As expected, this k coefficient is close to the slope characteristic of the elastic range. The limiting case is the infinitely elastic material for which $k = 1.315$;

– structural steel S 235 was chosen as an example for case c. Here the approximation reads $\varepsilon_{rs} = 2.403\varepsilon_{ext}$. The limiting case is the perfectly plastic material and it yields $k = 2.404$.

The slopes of the infinitely elastic and perfectly plastic materials appear as boundaries for the $\varepsilon_{rs} = f(\varepsilon_{ext})$ (relations in Fig. 12b).

Practical rules for the use of the above apparatus

Given some metallic alloy with an unknown plastic behavior, the present set-up allows to draw its work-hardening curves, at least in an approximate manner. The authors prescribe the following steps for the study.

i) At room temperature, it is possible to perform tensile tests on the set-up and to register $\sigma(\varepsilon_{ext})$. This suffices to distinguish between cases a, b and c. Indeed, only case a is considered below, been by far the most important for forming problems:

– provided the furnace has been let aside, the set-up allows to place a second extensometer on the gauge length of the test-piece. In this case, the curve $\sigma(\varepsilon)$ is precisely known at 20°C,

– if only $\sigma(\varepsilon_{ext})$ is available, the hardening curve can be approximated by $\sigma(\varepsilon) = \sigma(2\varepsilon_{ext})$.

Then, a way of obtaining a more precise result is to enter this $\sigma(2\varepsilon_{ext})$ curve as a data for the F.E. software and calculate the $\varepsilon_{rs} = f(\varepsilon_{ext})$ relation. It yields a more precise value of k and it may be slightly different from 2.

ii) At elevated temperatures, only $\sigma(\varepsilon_{ext})$ is available and work-hardening often diminishes beyond a certain strain, the consequence of it has been some rise in the slope of $\varepsilon_{rs} = f(\varepsilon_{ext})$. According to the degree of accuracy required, several strategies can be used:

– keep $\sigma(k\varepsilon_{ext})$ as the work-hardening curve. In this formula, k is the coefficient determined by the experiments at room temperature. This can lead to an underestimation of ε at large strains. It has little practical consequence since the curve is almost flat at this stage. Indeed, if $f(x) \approx C^{st}$, there is no point in determining x with accuracy;

– nevertheless, the obvious idea to refine the result is to use the method already mentioned for room temperature: enter the $\sigma(k\varepsilon_{ext})$ curve as a data in the F.E. software. It yields a relation $\varepsilon_{ext} = g(\varepsilon_{rs})$ which allows to calculate the $\sigma(g(\varepsilon_{rs}))$ curve. In the authors' experience, the difference from the $\sigma(k\varepsilon_{ext})$ curve is quite small.

4.2. Measurement of strain rate sensitivities by relaxation tests

A relaxation test consists of i) a tensile test which imposes an elastic strain ε, ii) a period of time in which ε is maintained constant while the stress decreases. Sometimes it drops to zero, sometimes it reaches a value which appears as a plateau on the graph $\sigma(t)$. Over time, the initially elastic deformation transforms, totally or partially, into a plastic one. Hence the viscous character of the transformation. Assuming the additive decomposition $\varepsilon = \varepsilon_e + \varepsilon_p$ (elastic+plastic deformations), derivation with respect to time yields $\dot{\varepsilon} = \dot{\varepsilon}_p + \dot{\varepsilon}_e = 0$ so that

$$\dot{\varepsilon}_p + \frac{\dot{\sigma}}{E} = 0, \tag{4.1}$$

where E is Young's modulus.

Along with tensile and creep tests, relaxation tests are the powerful means of investigating the warm and hot viscoplasticity of metallic alloys. Nevertheless, they are not as common as the previous ones. Lemaitre and Chaboche [8, p. 262] have collected some early experimental results. Recently, Prasad *et al.* [20] have used them to assess the ductility improvement of aluminum alloys and Yang *et al.* [21] have fitted the decrease in stress with exponential functions. The relaxation tests are well adapted to the study of service life expectancy: tur-

bine blades submitted to centrifugal forces, fasteners, nuclear reactor vessels in pressurized water reactors maintained during years at 290°C, not to mention heat exchangers.

Derivation of m, strain rate sensitivity, from the relaxation tests

The sensitivity to the strain rate was first introduced in forming problems. Consider, for example, wire drawing. At a given temperature, the stress necessary to the elongation of the wire raises with the drawing speed; hence the interest of:

$$m = \frac{\partial \operatorname{Ln} \sigma}{\partial \operatorname{Ln} \dot{\varepsilon}_p}, \tag{4.2}$$

where σ and $\dot{\varepsilon}_p$are measured in a steady state. In the case of relaxation, formula (4.2) can be specified as follows. Since $\dot{\varepsilon}_p = -\dot{\sigma}/E$ with $\dot{\sigma} \leqslant 0$:

$$m = \frac{\partial \operatorname{Ln} \sigma}{\partial \operatorname{Ln} |\dot{\sigma}|}. \tag{4.3}$$

A priori, m fluctuates with t. Nevertheless, the interest of the parameter is that it is approximately constant once a steady state is reached. It increases with temperature.

As stated in LEMAITRE and CHABOCHE [8, p. 264], at temperature a multiplicative form $\sigma = K\varepsilon_p^n \dot{\varepsilon}_p^m$ is often assumed for metals tested in tension with $\sigma(0) = 0$. Strain hardening is accounted for by the exponent n. In relaxation tests, $\sigma(0) = \sigma_0$ and there is no work hardening ($n = 0$). If m is constant in some period of time, the Appendix shows that $\sigma(t)$ takes the form of a power law of an exponent $-m/(1-m)$ which writes:

$$\log_{10}[\sigma(t) - \sigma_a] = m \log_{10}[\dot{\varepsilon}_p(t)] + c^{st}. \tag{4.4}$$

The Appendix gives details on how to smooth the relaxation curves affected by interferences and on how to check relation (4.4) in certain intervals of recording.

Experimental results

Relaxation tests were performed on the 2024 T3 alloy. The initial tension was done at a deformation rate of $2 \times 10^{-4}\,\mathrm{s}^{-1}$ to avoid creep during the elastic phase. Three initial stresses σ_0 were selected: 80, 160 and 240 MPa and four temperatures chosen: room temperature, 150, 250 and 350°C. Since 240 MPa is too much for 350°C (see Fig. 9), only eleven tests were recorded. The results appear in Fig. 13. All the curves $\sigma(t)$ present two phases. In Phase 1, the stress decreases rapidly from the initial σ_0. In Phase 2, the derivative $\dot{\sigma}(t)$ is much

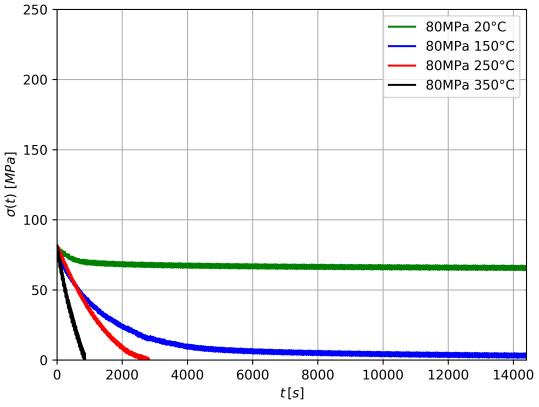

a) $\sigma_0 = 80$ MPa

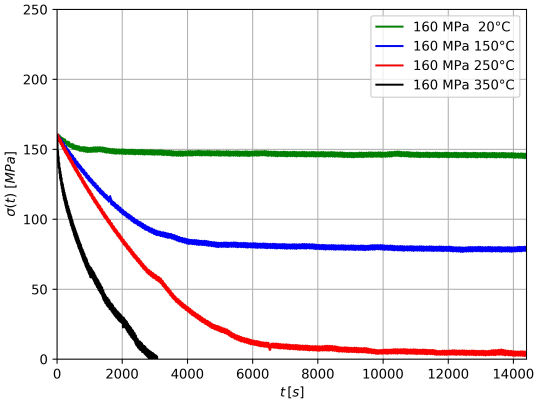

b) $\sigma_0 = 160$ MPa

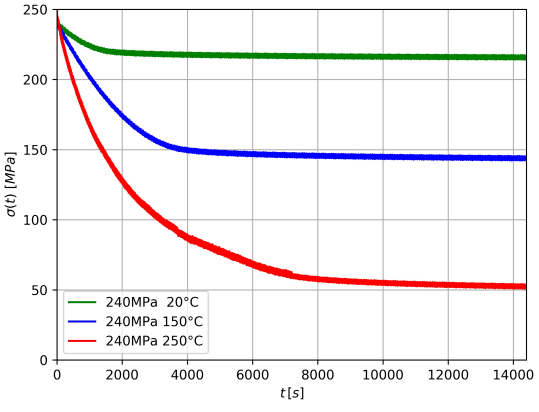

c) $\sigma_0 = 240$ MPa

Fig. 13. 2024 T3 alloy. Stress versus time for eleven relaxation tests.

smaller, although no asymptote could be determined. A parallel can be done with the primary and secondary phases of the creep tests, although the analogy may not be complete. The tests are presented in a period of four hours, because after that only straight, almost horizontal lines appear on the graphs. Phase 1 lasts between a quarter of hour and an hour and a half. Its duration increases with temperature. The data were recorded every 0.1 s and they are noised (see the Appendix). This can be attributed to electrical interferences. The discretization of the stress data is about 0.6 MPa and the typical noise is a variation of 0.6 or 1.2 MPa around a fitting line obtained by the least squares method.

For a given temperature, the form of the curves does not change much with σ_0. They are almost parallel for 80 and 160 MPa. The initial fall is somewhat more marked at 240 MPa. At any given time t, the stress is lower with increasing T and the deformation rate $\dot{\varepsilon}(t) = \dot{\sigma}(t)/E$ is consequently higher. $E(T)$ is given by Eq. (3.1).

The difference between Phases 1 and 2 can be quantified by calculating the apparent activation energy Q from the relaxation curves. This parameter measures the sensitivity of the material to the temperature along the deformation path. It intervenes in laws of behavior such as the one proposed by SELLARS and TEGART [22]. As exposed by MONTHEILLET [23, p. 233], in the case of forming problems, Q can be calculated either as:

$$Q = \left.\frac{\partial \operatorname{Ln} \dot{\varepsilon}}{\partial (1/T)}\right|_{\varepsilon,\sigma} \tag{4.5a}$$

or

$$Q = \frac{R}{m} \left.\frac{\partial \operatorname{Ln}(\Delta\sigma)}{\partial (1/T)}\right|_{\varepsilon,\dot{\varepsilon}}, \tag{4.5b}$$

where R is the perfect gas constant and T the absolute temperature. In relaxation tests, $\varepsilon = 0$. Thus (4.5.a) can be used with values $\dot{\varepsilon}$ taken at the same level of stress and (4.5.b) with values of σ taken at the same level of the strain rate. Hence:

– In a first step, the initial deformation rates $\dot{\varepsilon}(0)$ were considered. They happen to be close for the three σ_0, so that they have been averaged and depend only on the temperature. They appear in Table 3.

TABLE 3. Initial values of the deformation rates in relaxation.

T [°C]	20	150	250	350
$\dot{\varepsilon}(0)$ ($\times 10^{-6}\,\mathrm{s}^{-1}$)	0.31	0.63	1.36	2.08

According to Fig. 13, the calculation is possible between 150 and 250°C for $\sigma_0 = 160$ and 240 MPa. Formula (4.5a) yields $Q \approx 15\,\mathrm{kJ/mole}$, a value characteristic of the beginning of Phase 1.

– In a second step, the decreases $\Delta\sigma$ from the initial σ_0 were considered for common values of $\dot{\varepsilon}$. Formula (4.5b) was applied between 150 and 250°C for $\dot{\varepsilon}(t) = 10^{-7}\,\mathrm{s}^{-1}$ (at the end of Phase 1) and $\dot{\varepsilon}(t) = 5 \times 10^{-8}\,\mathrm{s}^{-1}$, $10^{-8}\,\mathrm{s}^{-1}$, $0.5 \times 10^{-8}\,\mathrm{s}^{-1}$ in Phase 2. This part of the $\sigma(t)$ curve being rather flat, no wonder that $\Delta\sigma$ varies little for these different rates. Strain rate sensitivity m was taken as the average between the values for 150 and 250°C (see Table 5 below), that is $m = 0.034$. With these assumptions, the result was $Q \approx 300\,\mathrm{kJ/mole}$.

Values of 100 to 400 kJ/mole are currently found when metals undergo transformations controlled by diffusion [23]. It is thus possible to say that:

– In Phase 2, some microstructural transformation takes place. This is typical of what happens in service conditions. The corresponding values of m can be compared to the values obtained by tensile and creep tests.

– In Phase 1, phenomena take place of a mechanical origin, they take place simultaneously. Just after the displacement of the movable crossbar has been stopped, there may intervene clearance compensation or alignment of the mounting balls. Proof of that is that the phenomenon appears at 20°C, although there is little microstructural activity at this temperature. The values of m can be calculated but they have no straightforward interpretation because of the mixed origin of the stress relaxation.

m values

To evaluate m, the following tools were chosen:

– the calculations were done in a Python environment,

– the Golay–Sawitzki smoothing was used in $\sigma(t)$ and allowed to calculate its derivative $\dot{\sigma}(t)$ (see Appendix for further details).

Results of the calculation of m in Phase 2

They appear in Table 4 as the result of the analysis of the eight curves for which the relaxation was not complete ($\sigma(t_f) = 0$ at $t_f = 14\,400\,\mathrm{s}$).

Table 4. Values of the strain rate sensitivity as a function of temperature.

T [°C]	20	150	250
m	0.015	0.028	0.040

Table 4 suggests the following remarks:

– m values are constant during Phase 2 in the range $\dot{\varepsilon} = 10^{-7}$ to $10^{-9}\,\mathrm{s}^{-1}$. They were calculated on three curves with different initial stress σ_0 for

$T = 20$ and 150°C and on two curves for $T = 250$°C. The results varied little with σ_0;

– In the literature, the authors could not find data on the 2024 alloy in the T3 temper but on other grades of aluminum alloys. As can be seen in FROST and ASHBY [24, Fig. 4.16], m values vary among aluminums, the higher have been found for grades of high purity. But on the whole, they are of the same order of magnitude. The reference which best fits the experiments of this paper was found in [8, pp. 260 and 264]. It gives $m = 1/N = 0.038$ at $T = 180$°C for an AU2GN and $m = 0.037$ at $T = 200$°C for a quenched and aged AU4G. At room temperature, LANGILLE [25, Fig. 10], who varied the rate of deformation in his tensile tests on grades of the 6000 series, found 0.10 to 0.15 in his up-charge measurements. ZENASNI [26] used torsion tests and found $m = 0.010$ at $T = 20$°C [25, Fig. I-4] and $m = 0.050$ at $T = 250$°C [25, Fig. I-6];

– It was not possible to measure the rate sensitivity at 350°C since the stress falls to zero prematurely. As already mentioned, m increases with rising temperatures. For example, CHOVET-SAUVAGE [27, page 69] found values around $m = 0.14$ for 6000 grades at 400°C.

As a summary, it can be said that:

– relaxation tests with the present apparatus gave values of m and Q for low deformation rates (e.g. $10^{-7}\,\mathrm{s}^{-1}$). This may be their distinctive advantage on work-hardening and creep tests, which do not reach such low values;

– in the case of aluminum, the range of temperature in which they could be measured did not exceed 300°C because σ_0 could not be raised over 240 MPa. Such a limitation would not be met with ferrite or copper, for example. Besides, temperature could have been raised up to 500°C with the aid of other heating resistors.

5. Conclusions

A simple thermomechanical gear has been mounted on a tensile-testing apparatus. Its characteristic feature is a two-shelled furnace which encompasses the test-piece. The extensometer is placed outside the heated zone. Heating relies on electrical resistances and, in the present case, does rise above 400°C. The temperature in the reduced section of the test-piece is perfectly homogeneous. The thermal steady state is attained in only one minute with a variation of less than 1°C. The furnace could be machined in an ordinary mechanical workshop so it can be adapted to test-pieces of various sorts, plates, sheets or rounded specimens (wires, rods and bars).

The relation between the global strain ε_{ext} recorded by the extensometer and the homogeneous strain ε_{rs} in the reduced section within the furnace is the key point in the use of the apparatus. In the elastic range, it has been

found to be $\varepsilon_{rs} = 1.315\varepsilon_{ext}$. This allowed to determine Young's moduli. In the plastic and viscoplastic ranges, the $\varepsilon_{rs} = f(\varepsilon_{ext})$ relations are close to straight lines. At large strains, for the considered geometry, the latter could be approximated by $\varepsilon_{rs} = 2\varepsilon_{ext}$ as a first approach. More precise results can be obtained using the F.E. software. All this allows the drawing of work-hardening curves $\sigma = g(\varepsilon, \dot{\varepsilon}, T)$. Indeed, an asymptotic behavior is expected for most of the test-pieces, since these are designed so that their deformation concentrates in their reduced section at large strains. Nevertheless, the $\varepsilon_{rs} = f(\varepsilon_{ext})$ relation must be recalculated for each form of test-piece and position of the extensometer.

The apparatus was also used for relaxation tests, in which there is no change in strain. These tests work down to low strain rates ($5 \times 10^{-8}\,\mathrm{s}^{-1}$), common in in-service conditions, beyond the reach of conventional creep tests. A method of derivation of the strain rate sensitivity from the curves of decreasing stress has also been proposed. The Appendix documents how it can be implemented in a Python environment.

The present article thus validates the performances of short, tight-fitting furnace configurations. The strain inside the oven can be calculated. Nevertheless, the set-up does not conform to one accepted practice. Standard ASTM 21 recommends that the knives of the extensometer should be directly attached to the gage length of the specimen. For this reason, the present apparatus may not be adopted for commercial verifications. For metrological purposes, specialized equipment should be preferred, as evoked with impulse excitation techniques for Young's moduli.

In the authors' opinion, the apparatus is a serviceable gear for laboratories dealing with the deformation of metals at elevated temperatures. Materials scientists can adapt it to their own needs using inexpensive, easily available components such as room temperature extensometers, while taking advantage of the fast rise and accurate maintenance in temperature of their test-pieces.

Appendix. Determination of strain rate sensitivities from relaxation tests

Assuming the multiplicative form of the flow rule $\sigma = K\dot{\varepsilon}_p^m$ with a constant m, some algebra yields:

$$m\frac{\ddot{\sigma}(t)}{\dot{\sigma}(t)} = \frac{\dot{\sigma}(t)}{\sigma(t)} \tag{A.1}$$

and $\sigma(t)$ can be integrated analytically as a power law. With a suitable shift in the origin of σ and t, it becomes:

$$\sigma(t) = \alpha + \frac{\beta}{(t - t_0)^{m/(1-m)}}. \tag{A.2}$$

Since

$$\dot{\varepsilon}_p(t) = -\dot{\sigma}(t)/E, \qquad \dot{\varepsilon}_p(t) = \frac{m}{1-m}\,\frac{b}{E(t-t_0)^{1/(1-m)}}.$$

Writing $\alpha = \sigma_a$ since it is a stress and choosing appropriately the origin of time, (A.2) takes the form:

$$\log_{10}[\sigma(t) - \sigma_a] = m \log_{10}[\dot{\varepsilon}_e(t)] + K \tag{A.3}$$

with

$$K = \frac{m}{1-m} log_{10}\left[\frac{m}{1-m}\frac{\beta^{\frac{1}{m}-1}}{E}\right].$$

Hence the fitting of a set $\{\dot{\varepsilon}(t_i), \sigma(t_i)\}$ requires the identification of three parameters α, β and m. This can be done in the Python environment according to the subsequent procedure.

A representative sample of the noise affecting the $\sigma(t)$ curves is given in Fig. A-1. The perturbations last typically from 100 to 200 s and develop in 1000 or 2000 acquisitions.

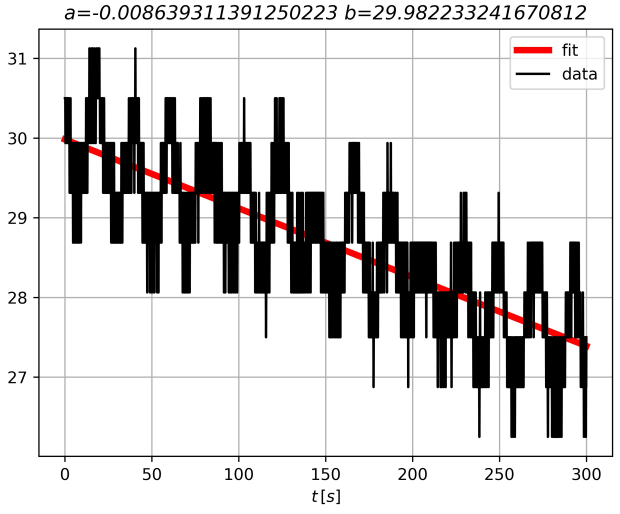

FIG. A-1. Noise on the $\sigma(t)$ curves.

Smoothing is necessary and the Golay–Sawitzky algorithm was chosen. Since no calculation of the curvature is needed, polynomials of the order 2 were used. The width of the window $2l + 1$ was taken as $l = 2000$, hence the use of the Python function Golay (4001,2). The derivation of the Golay smoothed curve is straightforward with the Least Squares fitting, which requires the analytical calculation of the Jacobian of the function:

$$f(x) = \alpha + \beta x^m, \quad \frac{f}{\alpha} = 1, \quad \frac{f}{\beta} = x^m, \quad \frac{f}{m} = \beta x^m \,\mathrm{Ln}(x). \tag{A.4}$$

This yields out α, β and m and can be illustrated with the example of the test performed from $\sigma_0 = 160\,\text{MPa}$ at 250°C (see Fig. 8b). The partition between Phases 1 and 2 takes place around $t = 6800\,\text{s}$, at $\dot{\varepsilon} = 3.15 \times 10^{-8}\,\text{s}^{-1}$, $\sigma = 9.45\,\text{MPa}$. On the log/log graph presented in Fig. A-2, Phase 1 is convex and Phase 2 concave, hence $m > 1$ for the first and $m < 1$ for the second phases.

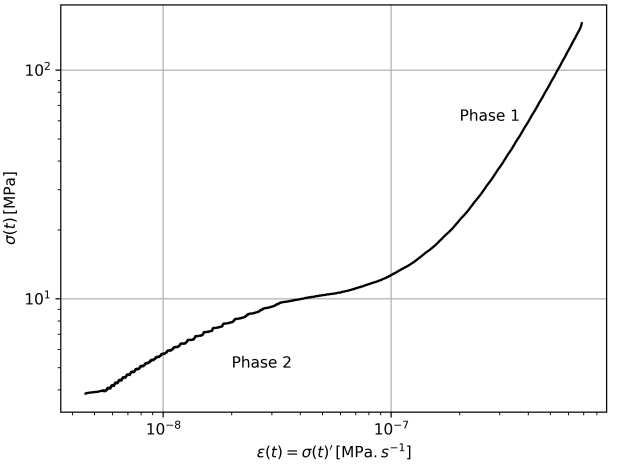

FIG. A-2. log-log representation of the cloud $\{\dot{\varepsilon}_k, \sigma_k\}$.

The fittings are quite tight as can be seen in Fig. A-3. $m = 1.75$ has no direct physical interpretation, for reasons pointed above. On the contrary, $m = 0.03975$ corresponds to a classical order of magnitude $m = 0.04$ of the rate sensitivity of 2024 T at 250°C.

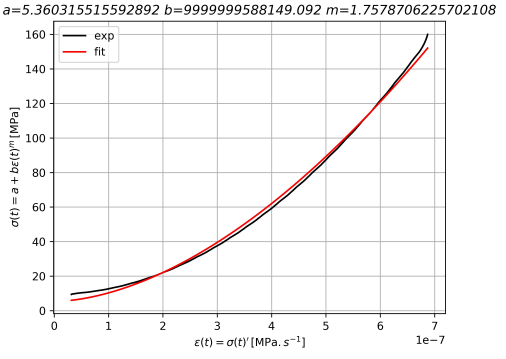

Phase 1: $m = 1.75787$

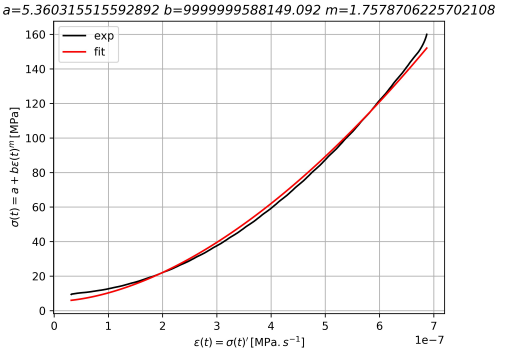

Phase 2: $m = 0.03975$

FIG. A-3. Fittings on the $\sigma(t)$ curves.

Acknowledgements

The authors are greatly indebted to Frank Montheillet, the French National Centre for Scientific Research (CNRS) senior scientist, emeritus, and to David Piot, fellow researcher with the Ecole Nationale Supérieure des Mines de Saint-Etienne (France) for the fruitful discussions which led to this article. They also benefitted from constant support of Séverine Girard, responsible for the machinery.

References

1. ASM Metal Handbook, Vol. 8, *Mechanical Testing and Evaluation*, H. Kuhn and D. Medlin [eds.], ASM International, Materials Park, OH 44073-0002, 2000.
2. F. MONTHEILLET, Ch. DESRAYAUD, *Essais rhéologiques à chaud (Rheological tests at elevated temperatures),* Techniques de l'ingénieur, **M3009**, June 2009.
3. D. FABRÈGUE, O. BOUAZIZ, D. BARBIER, *Nano-twinned steel exhibits high mechanical properties obtained through ultra-rapid heat treatment*, Materials Science & Engineering, A, **712**, 765–771, 2018.
4. J. CODRINGTON, P. NGUYEN, S.Y. HO, A. KOTOUSOV, *Induction heating apparatus for high temperature testing of thermo-mechanical properties*, Applied Thermal Engineering, **29**, 2783–2789, 2009.
5. *Standard Test Methods for Elevated Temperature Tension Tests of Metallic Materials*, ASTM E21, West Conshohocken PA: ASTM International, 2020.
6. D. ŻYMEŁKA, S. SAUNIER, J. MOLIMARD, D. GOEURIOT, *Contactless Monitoring of Shrinkage and Temperature Distribution during Hybrid Microwave Sintering*, Wiley online library, 2011.
7. P. LUONG, R. BONNAIRE, J.N. PÉRIÉ, Q. SIRVIN, L. PENAZZI, *Speckle Pattern Creation Methods for Two-dimensional Digital Image Correlation Strain Measurements Applied to Mechanical Tensile Tests up to 700° C*, Wiley online library, 2021.
8. J. LEMAITRE, J.L.CHABOCHE, *Mécanique des matériaux solides (Mechanics of Solid Materials)*, Dunod, Paris, 1996.
9. A. WERESZCZAK, M. FERBER, T. KIRKLAND, A. BAMES, E. FROME, M. MENON, *Asymmetric tensile and compressive creep deformation of hot-isostatically pressed Y_2O_3-doped – Si_3N_4*, Journal of the European Ceramic Society, **19**, 227–237, 1999.
10. J.M. Thomas, J.F. Carlson, *Errors in Deformation Measurements for Elevated Temperature Tension Tests*, ASTM Bulletin, ASTM, 47–51, 1955.
11. G. ROEBBEN, B. BOLLEN, A. BREBELS, J. VAN HUMBEECK, O. VAN DER BIEST, *Impulse excitation apparatus to measure resonant frequencies, elastic moduli, and internal friction at room and high temperature*, Review of Scientific Instruments, **68**, 12, 4511–4515, 1997.
12. *Standard Test Method for Young's Modulus, Tangent Modulus, and Chord Modulus*, ASTM E111, West Conshohocken, PA: ASTM International, 2017.
13. D.C. HOPKINS, T. BALTIS, J.M. PITARESS, D.R. HAZELMYER, *Extreme Thermal Transient Stress Analysis with Pre-Stress in a Metal Matrix Composite Power Package*,

Additional Conferences, Device Packaging HiTEC HiTEN & CICMT, January 2012, doi: 10.4071/HITEC-2012-THA25.

14. L.F. Mondolfo, *Aluminum Alloys: Structure and Properties*, Butterworths and Co. Ltd., London, p. 806, 1976.
15. G.B. Kim, J.L. Rempe, D.K. Knudson, K.G. Condie, B.H. Sencer, *In-situ creep testing capability for the advanced test reactor*, Nuclear Technology, **179**, 2012, doi: 10.13182/NT10-58.
16. *High Temperature Characteristics of Stainless Steels*, [in:] A Designer's Book Series, **9004**, Nickel Development Institute, 2007.
17. Z.L. Pan, N. Wang, Z. He, *Measurement of elastic modulus in Zr alloys for CANDU applications*, 11th International Conference on CANDU fuel, Niagara Falls, Ontario, CW-128700-CONF-001, October 17–20, 2010.
18. D.O. Northwood, I.M. London, L.E. Bähen, *Elastic constants of zirconium alloys*, Journal of Nuclear Materials, **55**, 3, 299–310, 1975.
19. S. Terzi, *Comportement à haute température du superalliage Udimet 720 élaboré par métallurgie des poudres et optimisé pour la tenue en fluage, (Behavior at high temperature of superalloy Udimet 720 produced by powder metallurgy and optimized for creep resistance)*, PhD Dissertation, Institut National Polytechnique de Toulouse, France, 2006.
20. K. Prasad, H. Krishnaswamy, J. Jain, *Leveraging transient mechanical effects during stress relaxation for ductility improvement in aluminum AA 8011 alloy*, Journal of Materials Processing Technology, **255**, 1–7, 2018.
21. J. Yang, H. Jiang, Z. Yao, J. Dong, *Limitations of calculating stress relaxation limit by function-fitting of Inconel 718 superalloy*, Materials Letters, **221**, 89–92, 2018.
22. C.M. Sellars, W.J. McG. Tegart, *Hot Workability*, International Metallurgical Reviews, **17**, 1, 1–24, 1974.
23. F. Montheillet, *Déformation à chaud des métaux: physique et mécanique (Hot deformation of metals: physics and mechanics)*, Ellipses, Paris, 2019.
24. H.J. Frost, M.F. Ashby, *Deformation Mechanism Maps: the Plasticity and Creep of Metals and Ceramics*, Pergamon Press, Oxford, 1982.
25. M. Langille, *Influence des constituants microstructuraux sur la formabilité des tôles en alliages d'aluminium, (Influence of the microstructural constituents on the formability of aluminum alloy sheet),* PhD Dissertation, Communauté Université Grenoble Alpes, France, 2019.
26. M. Zenasni, *Caractérisation expérimentale et modélisation du comportement du cuivre en grandes déformations : sensibilité à la vitesse (Experimental characterization and simulation of the behaviour of Copper at large strains : strain rate sensitivity)*, PhD Dissertation, Université de Metz, France, 1992.
27. C. Chovet-Sauvage, *Evolution des microstructures et des textures en grande déformation à chaud d'un alliage Al-Mg-Si, (Evolution of microstructures and textures at large strains of a hot worked Al-Mg-Si alloy)*, PhD Dissertation, Ecole des Mines de Saint-Etienne, France, 2000.

Received July 28, 2022; revised version April 26, 2023.
Published online 24 May, 2023.